SUPPLEMENTAL MATERIALS

p38 inhibition ameliorates skin and skull abnormalities in Beare-Stevenson cutis gyrata syndrome *Fgfr2*$^{+/Y394C}$ mice

Wang et al.

Supplemental Figures 1-6, Table 1, Methods, and References

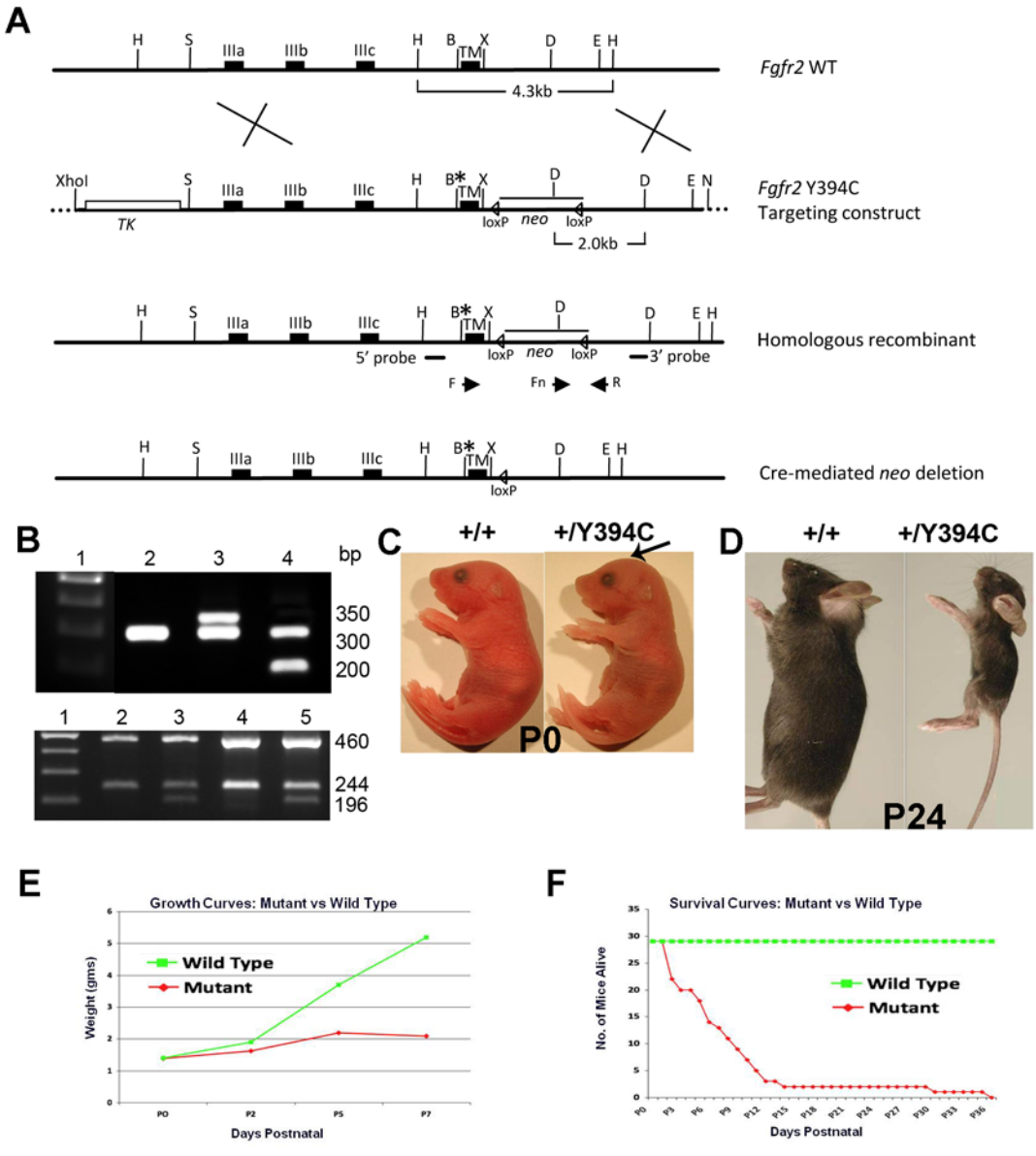

Supplemental Figure 1

Generation of *Fgfr2*$^{+/Y394C}$ mice. **(A)** The Fgfr2 targeting construct contains exons IIIa, IIIb, IIIc, and exon 10, which codes for the transmembrane domain (TM) of the gene, a neo cassette flanked by loxP sequences (open arrows), and the 1181A>G (based on nucleotide sequence NM_010207.2 and results in Y394C protein mutation) (*) in exon 10. Screening for recombinant clones was done by Southern blot analysis using restriction enzymes HindIII (H) or DrdI (D) and probes indicated (-). Other restriction enzyme sites noted are SacI (S), BsaHI (B), XcmI (X), and EcoNI (E). PCR primers (F, Fn, R; arrows) used for genotyping are shown. **(B)** (Upper panel) Genotyping results from PCR of tail DNAs. Lane 1: 100 bp DNA ladder; lane 2: wild-type +/+, 300 bp; lane 3: heterozygote +/Y394C [wild-type allele 300 bp and mutant allele after *neo* deletion with only one remaining loxP sequence, 350 bp]; and lane 4: heterozygote +/Y394C^{neo} [wild-type allele 300 bp and Y394C allele with *neo* cassette, 200 bp]. (Lower panel) RT-PCR results from PpuM1/Xho1 restriction enzyme-digest of *Fgfr2* alleles expressed in calvaria (lanes 2 and 3) and skin (lanes 4 and 5). Lane 1: 100 bp ladder; lane 2: wild-type +/+, 460 bp and 244 bp digestion products; lane 3: heterozygote +/Y394C [wild-type allele 460 bp, wild- type & Y394 allele 244 bp and Y394 allele 196 bp digestion products]; lane 4: wild-type +/+; lane 5: heterozygote +/Y394C. **(C and D)** Gross appearance of *Fgfr2*$^{+/Y394C}$ mice. **(C)** Note no significant difference in the body size (P0, +/Y394C [n=12] versus +/+ [n=9]: 1.402 ± 0.081 g versus 1.374 ± 0.122 g, *P*=0.5470) and limb length between the wild-type and mutant at P0. The mutant has a dome-shaped skull (arrow). **(D)** Note significant difference in the body size between the wild-type and mutant at P24. **(E and F)** Weight and survival curves of *Fgfr2*$^{+/Y394C}$ (red) and wild-type (green) mice. **(E)** Weights of mice with age show growth retardation in the mutant (e.g., P5, +/Y394C [n=8] versus +/+ [n=4]: 2.160 ± 0.261

g versus 3.400 ± 0.342 g, $P<0.0001$). **(F)** Survival curves show that almost half of the *Fgfr2*$^{+/Y394C}$ mutants died within 24-36 hours after birth; most died within 2 weeks.

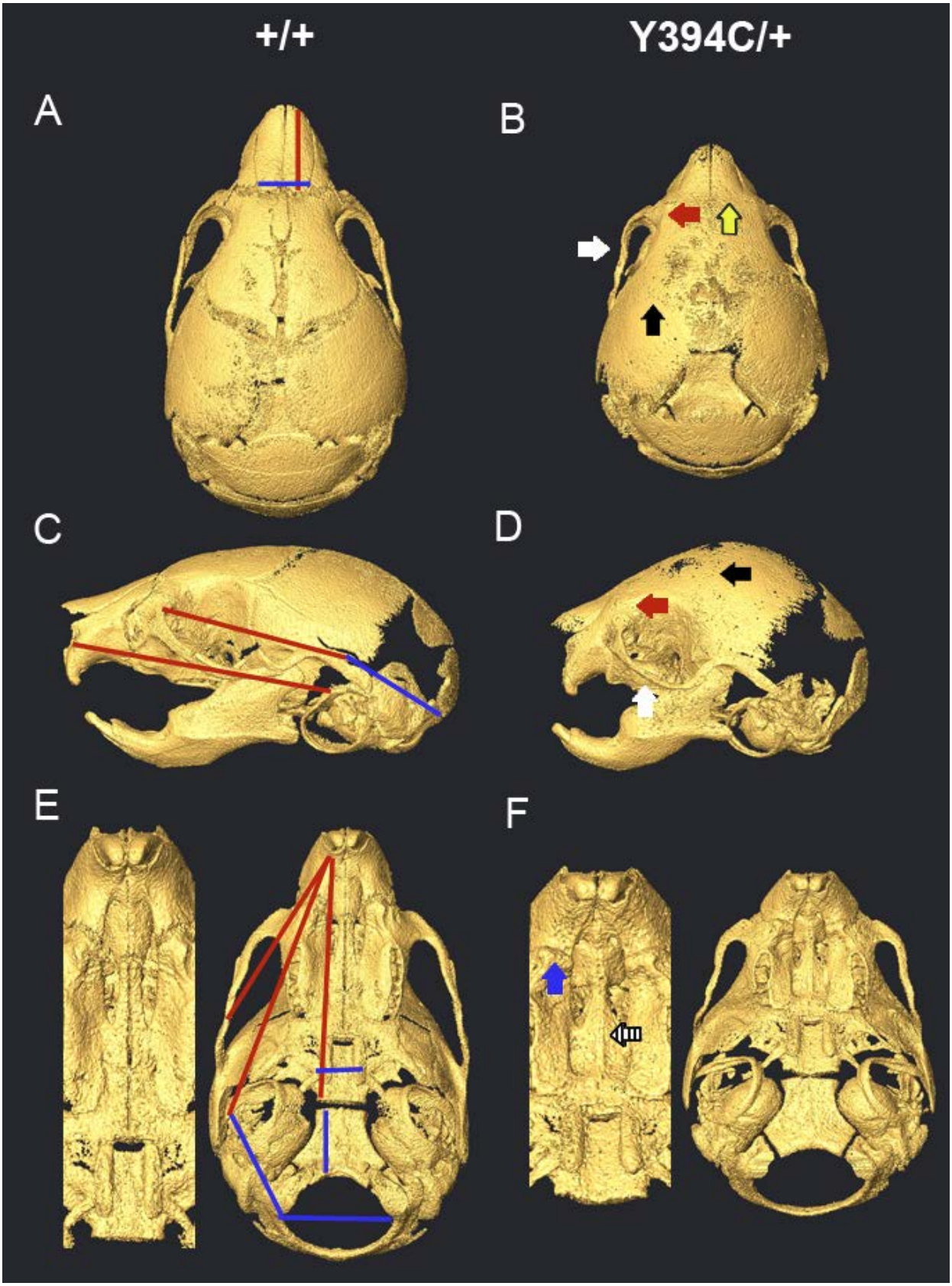
+/+
Y394C/+
A
B
C
D
E
F

Supplemental Figure 2

Micro-CT surface reconstructions of the skulls of *Fgfr2* $^{+/Y394C}$ mice at P8. **(A and B)** Superior views with nose upward. **(C and D)** Lateral views with nose to the left. **(E and F)** Inferior views with mandible removed, including close ups of the palate, nose upward (left). Distances between the length of the nasal bones, between the face and lateral vault, between the face and the petrous temporal bone, and between palate and the anterior cranial base are longer in the littermate controls relative to the mutants (**A, C, E;** red lines). In contrast, nasal width, sphenoid width, posterior cranial base length, dimensions of the petrous temporal, and posterior vault length are relatively shorter in the littermate controls (**A, C, E;** blue lines). Reported differences are, after scaling for overall differences in size, significant by bootstrap confidence intervals ($\alpha = 0.10$) following previously published methods (Lele and Richtsmeier. 1995; 2001). In mutants, coronal suture closure (**B and D**; black arrows) and the zygomaxillary suture closure are apparent (**B and D**; white arrows). The frontomaxillary (**B and D**; red arrows) and frontonasal suture (**B**; yellow arrow) are completely fused in mutants, while the premaxillary-maxillary suture (**F;** blue arrow) and intermaxillary suture (**F**; striped arrow) are more fused in mutants than controls (Supplemental Table 1).

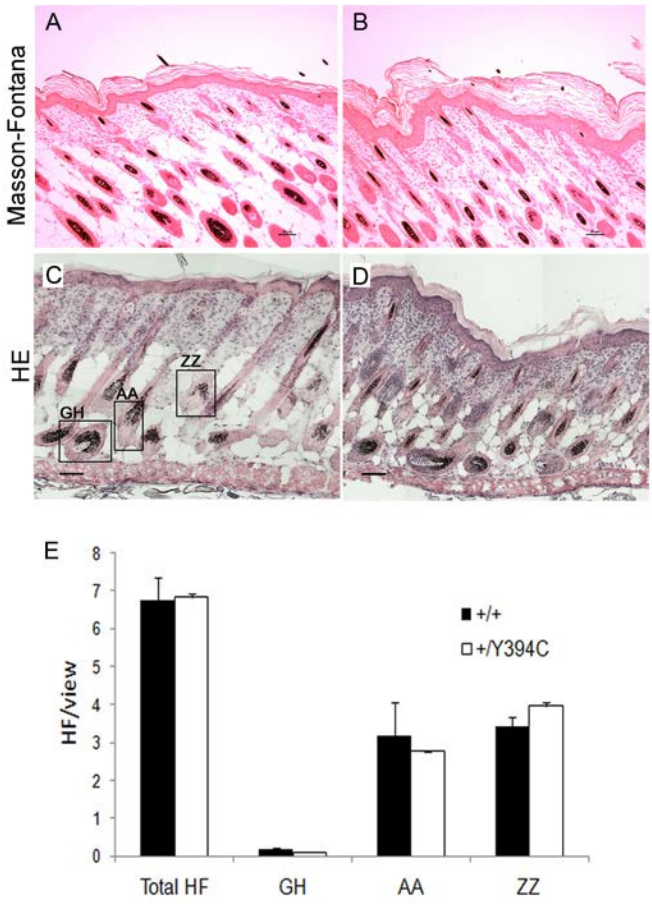

Supplemental Figure 3

Staining of melanin and quantification of hair follicles of *Fgfr2* $^{+/Y394C}$ mice at P5. (**A and B**) Masson-Fontana staining shows patchy melanin and dendritic melanocytes in the stratum basale. Most of the melanin and melanocytes were in the matrix of the hair follicles. **(C and D)** Hematoxylin Eosin (HE) shows hair follicles of 3 different types (Guard Hair, Awl/Auchenne and Zigzag) on skin from the back of *Fgfr2*$^{+/Y394C}$ and littermate controls. **(E)** Quantification of the total number of hairs and the number for each type shows no difference in the mutants as compared to the wild-type controls. More than 40 views were analyzed per mouse. HF: Hair Follicle; GH: Guard Hair; AA: Awl/Auchenne; ZZ: Zigzag. Scale bar=50 µm.

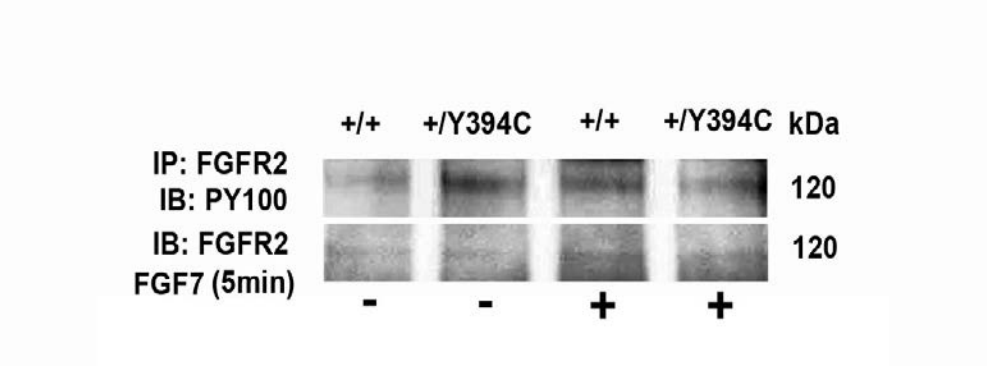

Supplemental Figure 4

The phosphorylated FGFR2 is elevated in the epidermal keratinocyte of *Fgfr2*$^{+/Y394C}$ mice. Keratinocytes from the epidermis of *Fgfr2*$^{+/Y394C}$ mice and wild-type controls were incubated in the absence or presence of 50 ng/ml of FGF7, lysed and immunoprecipitated with FGFR2 antibody. Blots were developed using phosphotyrosine antibody (upper panel) and FGFR2 antibody (lower panel). In the absence of FGF7, the Y394C mutant had increased phosphorylation and higher activity than that of the wild-type receptor.

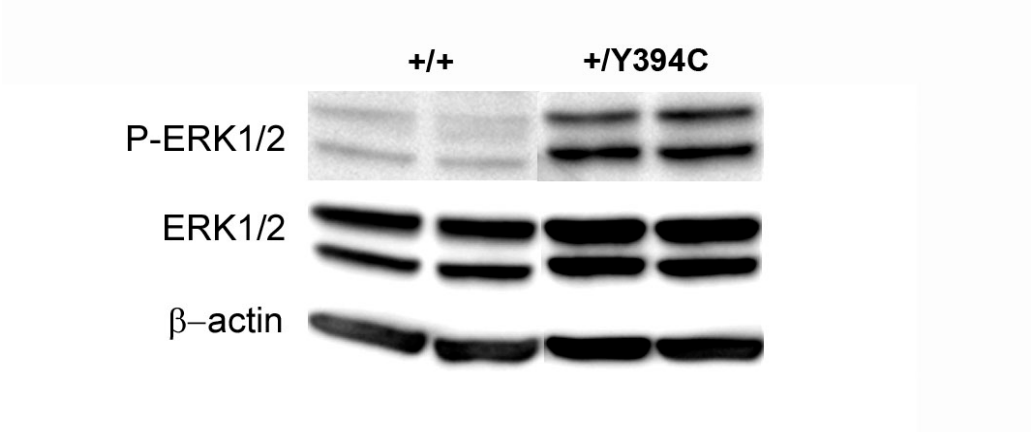

Supplemental Figure 5

The phosphorylated ERK1/2 is elevated in the skulls of *Fgfr2*$^{+/Y394C}$ mice.

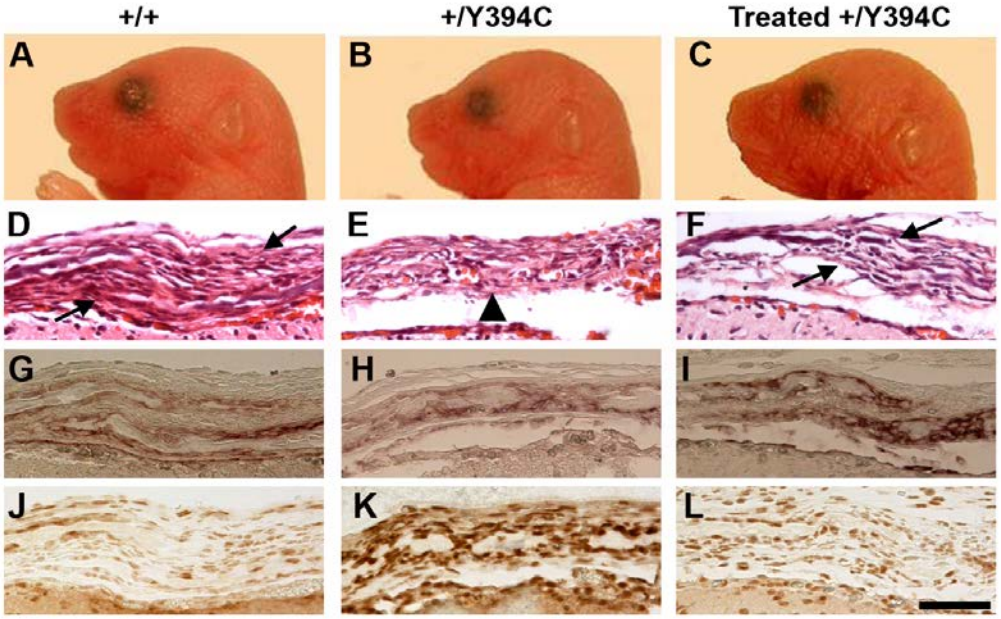

Supplemental Figure 6

In utero p38 inhibition attenuates skull abnormalities in one *Fgfr2*$^{+/Y394C}$ mice. **(A-C)** Heads of wild-type control, *Fgfr2*$^{+/Y394C}$, and p38 inhibitor-treated *Fgfr2*$^{+/Y394C}$ mice. Note the abnormal dome-shaped skull of the untreated mutant mouse **(B)** and moderate attenuation of the doming in the treated mutant mouse **(C)**. **(D-L)** Histological analysis by HE staining **(D-F)**, alkaline phosphatase activity **(G-I)**, and phospho-p38 immunohistochemistry **(J-L)** shows improvement of coronal suture morphology of the treated mutant mice **(F, I, L)** compared to untreated mutant mice at P0 **(E, H, K)**. Treatment of mutant mice with p38 inhibitor decreased the level of phospho-p38 in coronal sutures **(L)** to wild-type levels **(J)** compared to untreated mutants **(K)**. Arrows, osteogenic fronts; arrowhead, synostosis. (Scale bars: **D-L**=50μm).

Supplemental Table 1

Suture closure in Fgfr2$^{+/Y394C}$ mice at P0 and P8

	Fusion			
	P0		P8	
Sutures	+/Y394C (n=12)	Controls (n=9)	+/Y394C (n=10)	Controls (n=14)
	>=70% closed (total)*		>=70% closed (total)*	
Upper Coronal	12(12)	0(9)	8(10)	0(14)
Lower Coronal	1(12)	0(9)	10(10)	0(14)
Squamosal	8(12)	0(9)	4(10)	0(14)
Premax/Maxillary	4(12)	0(9)	10(10)	0(14)
Zygomaxillary	0(12)	0(9)	10(10)	0(14)
Zygomaticotemporal	0(12)	0(9)	4(10)	0(14)
Nasal/Frontal	0(12)	0(9)	10(10)	0(14)
Nasal/Premaxilla	0(12)	0(9)	0(10)	0(14)
Frontal/Maxilla	0(12)	0(9)	9(10)	0(14)
Internasal	0(12)	0(9)	2(10)	1(14)
Premaxillary	0(12)	0(9)	7(10)	12(14)
Intermaxillary	0(12)	0(9)	10(10)	0(14)

*<30% of suture patent, uni- or bilateral (total number of individual mice), as visualized from surface reconstructions of HRCT images.

Supplemental Methods

Generation of targeting construct and mutant mice as well as mutant allele genotyping. Two HindIII genomic subclones, one containing Fgfr2 exons 7-9 and the other with exon 10 were used to form the targeting construct. A ~5 kb SacI/HindIII (S/H) fragment from the 5' clone was inserted into the same restriction enzyme sites of pBlueScript II. The 3' HindIII subclone was digested with EcoNI (E) and blunted using T4 DNA polymerase followed by HindIII digest and this 4 kb fragment was ligated into the HincII/HindIII sites of the of the 5 kb BlueScript construct to give 9 kb of Fgfr2 sequence. A floxed neomycin cassette was inserted in the XcmI site. The Y394C mutation (analogous to the Y375C substitution in humans) was introduced into the construct by site-directed mutagenesis using complementary primers: forward 5'-gagatcacggcttcccctgattg**t***ctcgag*atagctatttactg-3', reverse 5'cagtaaatagctat*ctcgag*acaatcaggggaagccgtgatctc-3'. Underlined nucleotides were altered, those in bold change protein coding, and those italicized introduced an XhoI site. In the final construct there were 6.3 and 2.6 kb of homologous sequence 5' and 3' to the neomycin cassette. The final targeting vector was confirmed by sequencing, then linearized and introduced into R1 ES cells by electroporation. Positive cell clones were screened by Southern blot analysis using HindIII digestion with 5' probe and DrdI digestion with 3' probe. Male chimeras were generated and crossed with C57BL/6J females to achieve germline transmission of the mutant allele. The offspring were mated to generation N10 on the C57BL/6J background. Heterozygotes with neo (+/Y394Cneo) were mated with homozygous EIIA promoter Cre transgenic mice (EIIA-Cre, The Jackson Laboratory) to remove the neo cassette. Tail DNA was isolated by DNeasy tissue kit (Qiagen). The genotypes were determined by PCR analysis using primers from within *Fgfr2* exon 10 (forward primer F, 5'-

CACAAGCTGACCAAGCGCATCC -3'), intron 10 (reverse primer R, 5'-TGCCCATCCCACTGGGCAGCTC -3') and the neo cassette (forward primer Fn, 5'-TGTGTAGCGCCAAGTGCCCAGC -3'). Expression of the wild-type and mutant *Fgfr2* alleles was confirmed by using primers corresponding to the *Fgfr2* coding sequence of exons 5 and 10 (forward primer 5' -CAACACCGAGAAGATGGAG-3' and reverse primer, 5'-CCATGCAGGCGATTAAGAAG-3'. These generate a 704 bp PCR product from both alleles with a PpuM1 site at 460 bp. Additionally, the mutant allele contains an Xho1 site introduced by the site-directed mutagenesis primers at 656 bp. PpuM1/Xho1 digestion of the wild-type PCR product results in 460 bp and 244 bp fragments, while digestion of the heterozygous mutant PCR product results in 460 bp, 244 bp, 196 bp, and 48 bp fragments.

Care and use of mice for this study were in compliance with relevant animal welfare guidelines approved by Johns Hopkins University and Mount Sinai School of Medicine Animal Care and Use Committee.

Keratinocyte culture and in vivo FGFR2 functional study. Primary mouse keratinocyte culture was established following protocols provided by Dr. Soosan Ghazizadeh (Stony Brook University). Briefly, newborn Beare-Stevenson mouse pups were euthanized by hypothermia, skin epidermis was separated from dermis by floating skin on 0.25% trypsin overnight at 4ºC, and then minced and passed through a 70 μm cell strainer. The cell suspension was then seeded onto collagen-coated plates using Keratinocyte-Serum Free Media (KC-SFM) containing 0.3 mM calcium, and incubated at 34°C and 5% CO_2. 16-18 hours later, the media was changed to KC-SFM media containing 0.05 mM calcium and incubated at 34°C until the plates were 80-90% confluent in 3-4 days. Cultures were starved for 24 hours in KC-SFM media without Bovine Pituitary Extract (BPE) and human recombinant Epidermal Growth Factor (EGF) before

ligand treatment. To check for receptor phosphorylation, the keratinocytes were activated for 5 minutes with 50 ng/ml of FGF7 (one of the major ligands of FGFR2), lysed, immunoprecipitated with FGFR2 antibodies (Santa Cruz) and probed on an immunoblot with the PY100 antibody against the kinase domain. Two separate experiments from two litters of mice were performed to confirm the results.

Skin permeability assay. Skin permeability assay was performed as previously described (Hardman et al. 1998). In brief, freshly isolated embryos were rinsed in PBS and immersed in X-gal reaction mix (1.3 mM MgCl2, 100 mM NaPO4, 3 mM K3Fe(CN)6, 3 mM K4Fe(CN)6, and 1 mg/ml X-gal) in 50ml tubes. Embryos were incubated at 30^0C in a shaking incubator until color developed. Excess X-gal was removed by several thorough washes with PBS. Two litters of mice were observed at different developmental stages E14.5, 15.5, 16.5, and 18.5.

Supplemental references

Lele S, Richtsmeier JT. Euclidean Distance Matrix Analysis: confidence intervals for form and growth comparison. *Amer J Phys Anthropol*. 1995;98(1):73-86.

Lele S, Richtsmeier JT, eds. An invariant approach to statistical analysis of shapes. *Interdisciplinary studies in statistics series.* London, UK; Chapman and Hall-CRC Press; 2001

Hardman MJ, Sisi P, Banbury DN, Byrne C. Patterned acquisition of skin barrier function during development. *Development*. 1998;125(8):1541–1552.